Study of the acoustic emission response to a core-shell rubber-toughened, high-temperature composite

Swan, S. R., Devenport, T. M., Seraji, S. M., Griffin, J. M., Gashi, B. V., Creighton, C. & Varley, R. J.

Original citation & hyperlink:
Swan, SR, Devenport, TM, Seraji, SM, Griffin, JM, Gashi, BV, Creighton, C & Varley, RJ 2021, 'Study of the acoustic emission response to a core-shell rubber-toughened, high-temperature composite', Journal of Materials Science, vol. 56, no. 9, pp. 5609–5623.

DOI 10.1007/s10853-020-05612-4
ISSN 0022-2461
ESSN 1573-4803

Publisher: Springer

The final publication is available at Springer via http://dx.doi.org/10.1007/s10853-020-05612-4

Study of the Acoustic Emission Response to a Core-Shell Rubber Toughened, High-Temperature Composite

Samuel R. Swan[a], Timothy M. Devenport[b], Seyed Mohsen Seraji[a], James M. Griffin[b], Bekim V. Gashi[b], Claudia Creighton[a], Russell J. Varley[a*]

[a]Carbon Nexus at the Institute for Frontier Materials, Deakin University, Geelong, 3216, VIC, Australia
[b]Future Transport and Cities Institute, Coventry University, Coventry CV1, West Midlands, United Kingdom

* Corresponding author. russell.Varley@deakin.edu.au, Carbon Nexus at the Institute for Frontier Materials, Deakin University, 75 Pigdons Road, Waurn Ponds, Victoria, Australia 3216

Abstract

This work explores the effect of core shell rubber (CSR) addition on the cure reaction and resulting mechanical and thermal properties of a highly crosslinked network made from 4,4'- tetraglycidyl diamino diphenyl methane (TGDDM) and 3,3'-diamino diphenyl sulphone (DDS). Up to 20 wt% of a CSR rubber, composed of a soft polybutadiene (PBd) core and a hard poly methyl methacrylate (PMMA) shell was dispersed in the epoxy/amine and after cure was found to increase the glass transition temperature and thermal degradation temperatures modestly, while reducing the char yield. Flexural properties also reduced with CSR addition, although fracture toughness (K_{IC}) was increased by 45% at 20 wt% of CSR. Furthermore, the fracture strain energy release rate (G_{IC}) of the corresponding carbon fibre composite at the same CSR concentration, increased by almost 115%. Acoustic emission spectroscopy is introduced as a tool for investigating crack propagation during mode I loading and identifying any differences in the failure mechanism between the unmodified and the 20 wt% CSR modified carbon fibre composites.

Key words: Polymer-matrix composites (PMCs); High-temperature properties; Fracture toughness; Acoustic emission

1 INTRODUCTION

Although a wide range of polymer matrices are available for fibre reinforced composites, epoxy-based thermosetting resins are often used because of their overall balance of properties and versatile processing. The wide range of epoxy monomers and curing agents make it possible to formulate resins suitable for many service environments [1]. An area of interest within thermosetting resins is the higher temperature operating environment where long-term stability above 200 °C is desirable [2]. However, increasing thermal stability typically corresponds to increasing crosslink density which can deleteriously affect mechanical performance, such as embrittlement of the resin under high strain rate events [3]. From a molecular perspective, increasing thermal stability is typically achieved by restricting molecular mobility of the epoxy network, which requires increased aromaticity and/or functionality of the epoxy resin or amine monomers [4], [5].

Commercially, there are only a limited number of epoxy resin systems that have a high epoxide functionality and a sufficiently rigid network structure to achieve high temperature performance and durability above 200 °C. One such epoxy resin of interest is TGDDM, a commercially available monomer, that when cured with an aromatic hardener such as DDS, exhibits a glass transition temperature in excess of 250 °C. TGDDM-DDS based networks are commonly used for aerospace applications but tend to be brittle, resulting in a significant body of work focused on their toughening, using additives such as rubbers, thermoplastics and inorganic modifiers to name the most common [6]–[15]. High functionality resins such as TGDDM, generally show limited toughenability using traditional modifiers [16]–[18] due to the inability of the polymer network to undergo shear band formation and yielding. Regardless, if toughening can be achieved, it often corresponds with a decrease in strength, stiffness and processability.

The use of pre-formed core shell rubber particles as modifiers however, have shown excellent improvements in toughness for di-functional or less cross-linked epoxy network with minimal impact on glass transition and other desirable properties [19]–[24]. Core shell rubbers (CSR) are sub-micron particles with mean diameters between 50-100 nm which can be readily dispersed into common epoxy resins. They typically consist of a rigid thermoplastic shell of the order of 20 nm thick and an elastomeric core. Toughening occurs when a isostatic tensile load induced by the approach of a crack tip causes the CSR to cavitate, forming shear bands which absorb some of the energy from the fracture event and enhance toughness [19], [25]–[29].

However, while many studies have used CSR to successfully toughen epoxy resins, very few studies have explored highly cross-linked networks such as those based upon TGDDM. Indeed, Bradley et al showed that amongst three systems with T_gs between 189-225°C the core shell toughening response was absent [31]. Previous work on epoxy networks has indicated an inverse correlation between effective toughening and the bulk resin thickness relative to the crack front [26], [32], [33]. It is of interest therefore to understand not only the effect of CSR on the resin properties for highly crosslinked networks, but also on the toughness of the corresponding carbon fibre reinforced composite. An example of the limited studies using CSR to toughen epoxy composites, is that of Riew et al who showed that a TGDDM/DGEBA epoxy resin blend cured with the aromatic amine 44 DDS increased fracture toughness (G_{IC}) of the composite 45 %, from 500 J/m^2 to 890 J/m^2 [30].

Acoustic emission (AE) spectroscopy is a non-destructive testing and evaluation technique that combines high sensitivity, a large dynamic range, and a passive sensing nature. That is, it can detect external events or stress waves that occur across a wide frequency band. Already, the study of AE has enabled near-continuous monitoring of mechanical events governing failure in metals and composites. The extensive amount of research into AE for damage monitoring has led to a series of reports that have defined the frequency range of the main composite failure modes: matrix cracking (100-250 kHz), interlaminar and interply failure (250-420 kHz), and fibre failure 420-700 kHz [34]–[39]. The AE output however, is very computationally intensive such that various signal-processing approaches have been developed to predict crack length in the composite [40], utilize pattern recognition of the signal amplitude for fatigue life predictions [37], and predict the onset of damage [41], [42].

An area of interest that has not been widely exploited is the role AE can have in studying how the failure mechanism may be influenced by changes to a constituent material in the composite. A study by Lissek *et al*. compared the fracture of two different epoxy prepregs cured by compression moulding and autoclave consolidation and was able to show that the AE response varied according to the level of toughness of the matrix [40]. Also, Arnautov et al. studied a polyethersulfone (PES) toughened di-functional epoxy resin cured with an aliphatic hardener, and showed that the accumulated counts and peak amplitudes within the AE signal reduced between the neat resin and those modified by PES addition [43]. This was attributed to the accumulation of more defects in the modified resin prior to failure potentially indicative of the activation of thermoplastic toughening mechanisms within the polymer network.

Given the multi-spectral responses to different types of failure mentioned above, AE sensing of mechanical test data therefore, has the potential to provide new insights into the mechanisms of failure for both toughened and un-toughened systems. In this work, the effect of CSR particle addition on the fracture toughness of a highly-crosslinked TGDDM-DDS resin was studied both in the form of the cured resin and as a unidirectional carbon fibre composite. The influence of CSR addition to the cure of the epoxy network was studied by differential scanning calorimetry (DSC) and near-infrared spectroscopy (NIR). The thermal and mechanical properties of the neat resin were characterized by thermogravimetric analysis (TGA), dynamic mechanical thermal analysis (DMTA), and 3-point flexural testing. Single end notched beam (SENB) measurements were used to determine the K_{IC} fracture toughness of the resin, while dual cantilever beam (DCB) measurements determined the mode I inter-laminar fracture energy (G_{IC}) in parallel with acoustic emission spectroscopy. Analysis of the fracture surface was performed using scanning electron microscopy (SEM) for the neat resins and composite specimens. The time-based AE signal from Mode I fracture tests of unmodified and 20 wt% CSR modified composites was decomposed into frequency domains to determine the unique signature of failure modes determined from analysis of the peak frequencies.

2 EXPERIMENTAL METHODS

Neat epoxy resins were prepared from 4,4'-tetraglycidyl diamino diphenyl methane ((125.5 g-eq^{-1}) Araldite MY720, Huntsman Corp., USA) and cured with a 1:0.95 stoichiometric amount of 3,3'-diamino diphenysulfone (DDS) ((62 g-eq^{-1}) Tokyo Chemical Industries, JPN). The core shell rubbers were provided by Kaneka Corporation of Japan and are pre-dispersed by the proprietary MX^{TM} process into an epoxy master batch marketed under the Kane-Ace brand. Kane-Ace MX416 consists of CSR particles with a 50-70 nm diameter. These particles consist of a polybutadiene rubber and a PMMA core which is dispersed in a TGDDM (148 g-eq^{-1}, Araldite MY721) resin at a concentration of 25 wt% (±1 %). The unmodified TGDDM was then used to dilute the master batch and achieve a particle concentration of 2.5, 5, 10, 15, and 20 wt% CSR in epoxy. The amounts of each material used are provided in Table 1.

Table 1 - Composition of the monomer constituents for the neat resin formulations

	Mol. Weight	EEW (AEW)	Mass (g)					
TGDDM	502	125.5	100	90	80	60	40	20
MX416	592	148	0	10	20	40	60	80
DDS	248	(62)	49.40	48.65	47.90	46.40	44.9	43.4
wt% CSR in epoxy			0	2.5	5	10	15	20

To prepare the resin formulations, a rotary evaporator equipped with a heated silicon oil bath was used to degas and mix the resins concurrently. The MY720 and MX416 were placed into a round bottom flask and mixed under vacuum while heating at 120 °C for one hour. After sufficient degassing of the mixture, DDS was added and the mixture was stirred for a further 30 minutes.

Silicon moulds consisting of 13 x 6 x 54 mm and 13 x 3 x 65 mm cavities were placed in a convection oven and pre-heated to 120 °C. The resins were then quickly transferred to the moulds. A cure schedule of 2 hours at 120 °C, 2 hours at 150 °C and 2 hours at 180 °C followed by a free-standing post-cure for 2 hours at 205 °C was used for all resin formulations.

Composite laminates were fabricated from pre-impregnated carbon fibre tape. The epoxy-amine resin (75 g) was dissolved in dichloromethane (200 mL) and acetone (100 mL) by rigorous stirring until the mixture was a transparent yellow in the case of the unmodified resins, or a slightly opaque light pink for the core-shell modified variant. The carbon fibre was a standard modulus, 300 $g.sqm^{-1}$ unidirectional tape. The dissolved resin was wound through a manual infusion device onto a spool which was then placed in a ventilated drying oven at 45 °C for one hour followed by 75 °C for 30 minutes to remove the solvent. A total of 16 plies were used for each panel. A thin PTFE release film was inserted into the panels between the mid-plies at both ends of the laminates to act as a pre-crack. The lay-ups were vacuum-bagged, debulked, and cured on a hydraulic press pre-heated to 120 °C and applied pressure of 6.5 bar. The cure schedule for the neat resins and composites were the same with the exception that the composite laminates were debagged and post-cured in a convection oven. The laminates were 3.8 mm nominal thickness after cure and eight specimens were cut to nominal dimensions of 21x150 mm from each of the laminates.

Glass transition temperature (T_g) was evaluated by dynamic mechanical analysis on a Q200 DMA (TA Instruments, USA). A double cantilever apparatus was used to heat 65 mm long samples from 50 to 295 °C at a rate of 5 °C/min, while applying a frequency of 1 Hz and a displacement of 50 μm. The extrapolated onset of the decrease in the storage modulus, E', and the peak in the tan δ spectrum were used to establish the T_g of the cured network. Dynamic differential scanning calorimetry (DSC) was performed on the uncured resins for a series of five heating rates from 2.5°C/min to 20°C/min using a Polyma DSC200 (Netzsch GmbH, Austria). The model Kissinger and Flynn-Wall-Ozawa kinetic models were derived from DSC data to assess the effect of CSR addition on cure. Near infrared spectroscopy (NIR) was used to qualitatively evaluate the hydroxyl, secondary amine and epoxide groups after cure and post-cure on an Alpha FTIR spectrometer (Bruker Corp., USA). Spectra were collected at a resolution of 2 cm^{-1} and averaged over 64 scans across a spectrum from 7500 to 4000 cm^{-1}. Thermogravimetric analysis was performed on a Q50 TGA (TA Instruments, USA). Approximately 10 mg of cured resin was placed in a platinum crucible then heated in the chamber from 20-600 °C at a rate of 5 °C/min. Physical densities were studied by helium gas pycnometry on an Ultrapyc 1200e (Quantachrome Instruments, USA). Nominally, 2 grams of cured resin were weighed to the nearest 0.01 of a gram and the resin was placed in the pycnometer chamber. A series of pressurizations and purges were then performed and the final density was taken as the resulting average from all scans.

Flexural properties of the neat resin were carried out in accordance with ASTM Standard D790 [44] on an Instron (ITW Inc., USA) servo-electromechanical load frame in 3-point bending with a beam length of 48 mm. Properties were determined from an average over five samples Fracture toughness was assessed by single-edge notch flexural (SENB) testing according the ASTM Standard D3037 [45]. The pre-crack cavity was cut into samples and a pre-crack inserted using a small jeweler's hammer and a fresh razor blade for each sample.

The mode I strain energy release rate (G_{IC}) of the composites was measured by the double cantilever beam method according to ASTM Standard D5528 [46]. The loading rate was 1 mm/min. A high definition digital camera was used to track the crack tip front. The compliance calibration method was utilized to determine the value of fracture energy based on the load and displacement recorded at the servo-electromechanical load frame relative to the crack propagation in the sample.

The acoustic emission apparatus consisted of a Micro-II data acquisition unit, two voltage pre-amplifiers, two 20 mm diameter ceramic wide-band acoustic emission sensors and associated waveform

extraction software (Mistras Group Inc., USA). The amplification to each sensor was maintained at 20 dB with a 35 dB threshold. The AE sensors have an operational range between 70 kHz to 1 MHz and were placed along the centerline of the top face of the DCB specimens. Sensors were coupled to the surface by use of a polypropylene double-sided tape of 220 µm nominal thickness (tesa 51970 SE, Germany). The arrangement of DCB samples with AE sensors is shown in Figure 1.

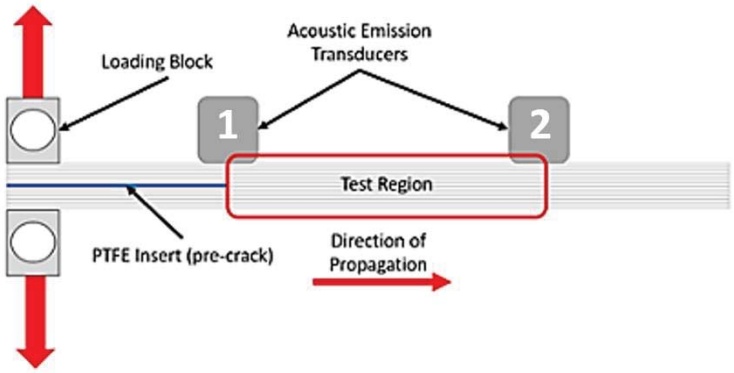

Figure 1 - Diagram of AE sensors onto DCB specimens for fracture toughness characterization

The attenuation of the sample material affects the propagation of soundwaves as the density of the material changes. That includes changes to material thickness and distance between the source and the sensor. The leading sensor (#1) was kept centered over the pre-crack tip and the lagging sensor (#2) placed 55mm from the crack tip. Each was aligned down the lengthwise centre of the beam.

Prior to each test, an automatic sensor test (AST) was carried out to assess the contact between sensor and sample and compare the sensitivity of sensor 1 to sensor 2 before and after testing. The AST sends a prescribed pulse from one sensor that is received by the other sensor. The output of this test displays the amplitude and hits of the sending and receiving sensors and the contact is considered good if at least 50% of the sent signal is received. Between sensors 1 and 2, the average received signal from a 96 dB nominal pulse amplitude was 58.33 dB (±6.62) and 59 dB (±5.87), respectively. Post-test, the average was 52 dB (±3.21) and 52 dB (±4.00), respectively. The cumulative drop in received signal from both sensors corresponded to a 10.1% decrease at the end-of-test state which is attributed to the reduction in laminate thickness after crack propagation.

3 RESULTS & DISCUSSION

3.1 Cure Kinetics, Glass Transition and Thermal Stability

Dynamic differential scanning calorimetry was carried out for the unmodified and 20wt% resin systems only and compared to each other. By increasing the ramp rate and applying Arrhenius modeling, the apparent activation energy was determined from peak temperature of each thermogram. While a number of methods exist to model the kinetics of these reactions, two very common ones, the Kissinger and Flynn-Wall-Ozawa models have been used here.

The Kissinger method is given as:

$$\ln\left(\frac{\beta}{Tp^2}\right) = \ln\left(\frac{AR}{Ea}\right) - \ln\left(\frac{Ea}{RTp}\right) \quad \text{(Eq. 1)}$$

where β is the heating rate, T_p is the peak exothermic temperature, R is the universal gas constant taken as 8.314 kJ/mol-K, A is the pre-exponential factor, and E_a represents the apparent activation energy.

The Flynn-Wall-Ozawa (FWO) method is often used in conjunction with the Kissinger method to verify the apparent activation energy. The method assumes the exothermic characteristics are equal across different heating rates and is as follows:

$$\ln(\beta) = \ln\left(\frac{AE_a}{Rf(\alpha)}\right) - 2.315 - 0.4567\,\frac{E_a}{RT_p} \quad \text{(Eq. 2)}$$

where it is assumed that values for the conversion, α, at each exothermic peak are equivalent between heating rates. The linear relationship of the heating rate to the reciprocal of peak exothermic temperature provides the activation energy from the slope of the line from increasing heating rates.

The thermograms for the modified and 20wt% modified resin systems shown in Figure 2 display a typical exothermic response during epoxy amine cure that increases in magnitude and T_p with increasing ramp rate as expected. A summary of the kinetic analysis are shown in Table 1 which highlight that CSR addition reduces the T_p yet increases the enthalpy of reaction. The activation energy barriers to reaction were determined to be 61.2 kJ/mol (Kissinger) and 69.4 kJ/mol (FWO) for the unmodified resins and 66.8 kJ/mol (Kissinger) and 75.0 kJ/mol (FWO) for the 20 wt% CSR modified, indicating an increase of about 5.5 kJ/mol regardless of model [47], [48]. The modest acceleration of the reaction as evidenced by the lower T_p and consistently higher enthalpies (after normalization) suggests surface catalyst of the reaction by the CSR particles. Despite this acceleration, higher activation energy

for the 20wt% CSR modified system likely reflects a comparatively restricted mobility or steric hindrance caused by the sub-micron scale particles in the glassy state. An accelerated effect has previously been reported for CSR modified epoxy resins [49], [50].

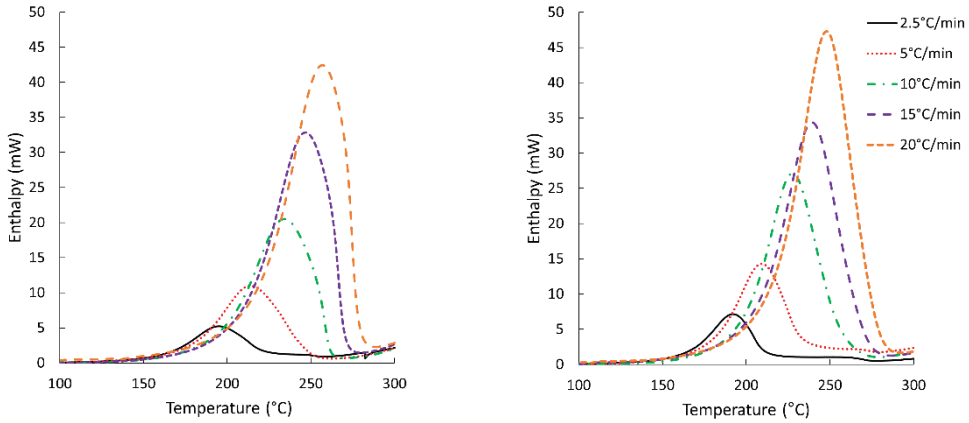

(a) (b)

Figure 2 - DSC thermograms of uncured resins for (a) the unmodified 0 wt% CSR and (b) the 20 wt% CSR formulations

Table 2 - Summary of peak temperature, enthalpies, and activation energies for neat resins studied by differential scanning calorimetry

	Heating Rate (°C/min)					Kissinger	FWO
0 wt% Un-modified	2.5	5	10	15	20	Ea (kJ/mol)	Ea (kJ/mol)
T_p (°C)	194.79	213.99	234.23	246.81	256.83	61.2	69.4
ΔH (J/g)	474.12	571.90	477.00	540.4	481.8		
20wt%							
T_p (°C)	191.82	209.66	227.63	239.26	247.94	66.8 (5.6%)	75.0 (5.5%)
ΔH (J/g)	587.63	634.63	654.25	585.38	591.25		

The T_g, as determined by DMA shown in Figure 3 and Table 2, exhibited a modest but consistent increase with increasing concentration of CSR as measured by the extrapolated onset of E' and the peak in the tan δ spectra, likely due to increased chemical interactions between the CSR and polymer matrix, as previously suggested. In addition to this modest increase in T_g, the magnitude of the tan δ peak also decreased somewhat with increasing CSR concentration, albeit erratically, reflecting restricted mobility around the CSR dispersed particles. Another observation from the traces is that, the storage modulus, again despite being somewhat erratic shows

an overall decrease with increasing CSR concentration due to their inherently lower modulus. Concurrent with a decreased storage modulus is a decrease in the physical density. Previously, investigations into DGEBA-based resin systems have reported similar reductions in storage modulus and minor increases to the T_g with CSR addition [51], [52] which has been associated with good dispersion of the particles in the cured resin [22], [23], [53]. Whilst the tan δ spectra was incomplete, from as much as could be determined, it appeared mostly symmetrical or unimodal suggesting a homogeneous network, at least on the microstructural level.

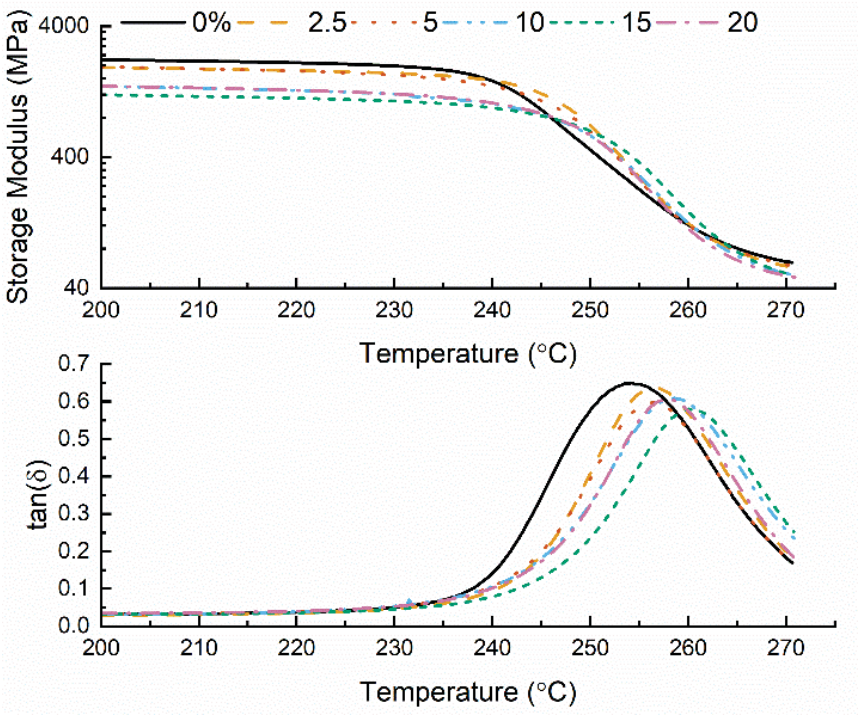

Figure 3 - Scans from dynamic mechanical analysis showing (a) storage modulus and (b) tan(δ) relative to ramp temperature

The thermal stability of the cured networks was also investigated using TGA, as measured by the onset of degradation (T_d) and the char yield (%) as shown in Table 2. Despite somewhat scattered and modest trends, it is still clear that the T_d increased while the char yield decreased with increasing CSR concentration. The increase can be attributed to an increase in cohesive strength arising from the epoxy CSR interactions, while the reduced char yield reflects the reduced thermal stability of the CSRs themselves.

Table 3 - Summary of glass transition, degradation temperatures, and char yield for the neat resins

	CSR WT%					
	0	2.5	5	10	15	20
T_g by E' ext. onset [and peak in tan(δ)] (°C)	238 [254]	244 [256]	246 [258]	244 [256]	249 [260]	246 [258]
T_d (ext. onset) (°C)	334	351	346	336	355	360
Char yield (wt%)	25.5	20.4	23.6	26.3	20.4	18.9
Cured resin density (g/cm^3)	1.283	1.251	1.229	1.219	1.212	1.198

Near infrared spectroscopy (NIR) was used to gain insight into the cure mechanism of the epoxy amine reaction, particularly during later stages of cure and to explore the impact of CSR on cure conversion. The NIR spectra of all the modified resins are shown in Figure 4(a) which show similar behavior, suggesting that the mechanism is relatively unaffected by the addition of the CSRs. The regions of interest, namely the epoxide (just under 4500 cm^{-1}), secondary amine (about 6600-6800 cm^{-1}) and hydroxyl peaks (7000-6900 cm^{-1}) are more closely examined in Figure 4(b) and 4(c) for the unmodified and 20 wt% CSR modified systems only. Figure 4(b) shows qualitatively that CSR addition produces a very small reduction in the extent of cure which can be attributed to the increased steric hindrance effects of the CSRs. The secondary amine and hydroxyl region, again, whilst mostly very similar for different CSR concentration, does possibly show some effect with increasing CSR addition. Figure 4(c) whilst comparing the unmodified and 20 wt% CSR system, shows that there is a modest increase in the secondary amine peak and decrease in the hydroxyl peak. Again, whilst being very minor, this suggests to a greater degree of etherification at higher CSR concentrations.

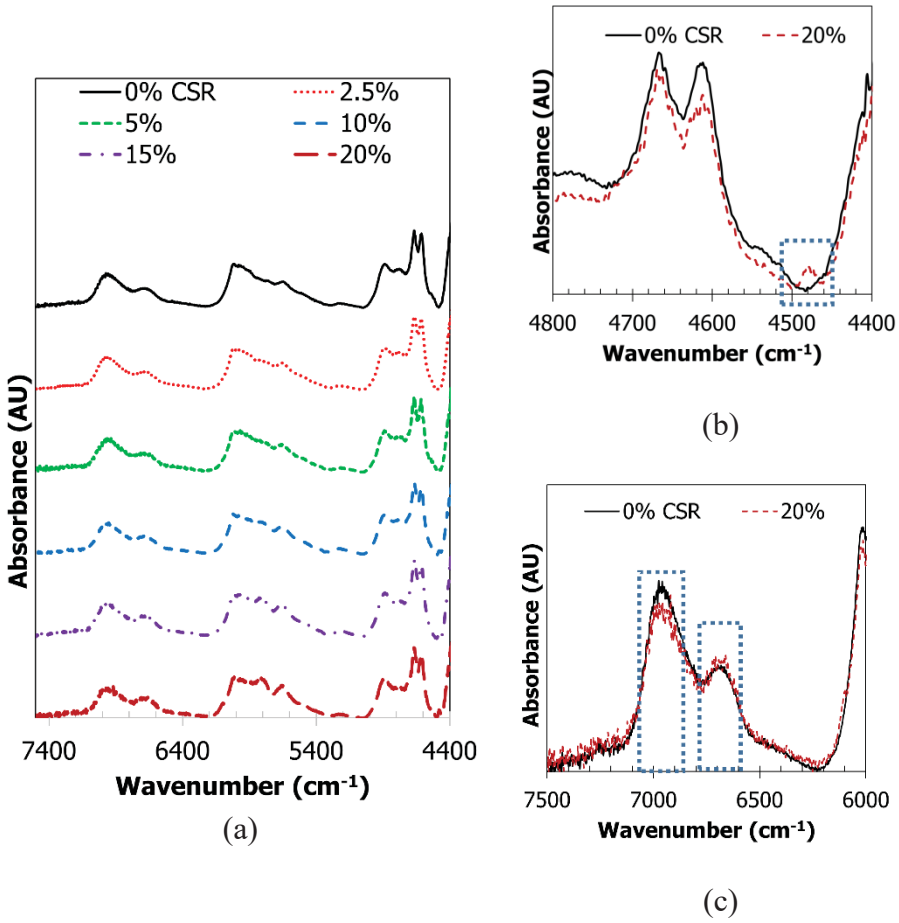

Figure 4 - NIR of (a) fully cured TGDDM-DDS from 0-20 wt% CSR loading and (b-c) the unmodified and 20 wt% for epoxide, hydroxyl, and primary/secondary amine peaks

3.2 Flexural and Fracture Properties of the Neat Resins

The mechanical and fracture properties of the neat resins shown in Figure 5 indicate a consistent decrease in flexural strength and modulus but an increase in fracture toughness with increasing CSR concentration. Despite the hard outer shell of the CSR, the core material is a polybutadiene rubber, so a reduction in stiffness is consistent with inclusions of mechanically weaker additives [54]. No discernible trend is observed for the strain to failure, likely due to the brittle nature of the epoxies and so less related to the presence of CSR regardless of concentration. In contrast, the fracture toughness while not showing any improvement in toughness at low levels of addition, did show a modest increase in K_{1C} from 15 wt% to 20 wt% CSR addition. The improvement to average fracture toughness was 11.4% for 15 wt% of CSR and 45.0% for the 20wt% CSR samples. It is important to note that the high level of CSR required to achieve significant improvements in fracture toughness is not typical. As discussed earlier, CSRs have

been shown to impart very large improvements to toughness in epoxy networks either at much lower concentrations [22], [24], [52] or toughened to orders of magnitude higher than the pure epoxy [23], [53], [55]. Importantly however these results were not for very high crosslink density networks as discussed here, where the crosslink density restricts complementary toughening mechanisms such as matrix shear yielding [19], [21] from occurring in conjunction with the CSR particle cavitation and crack bridging.

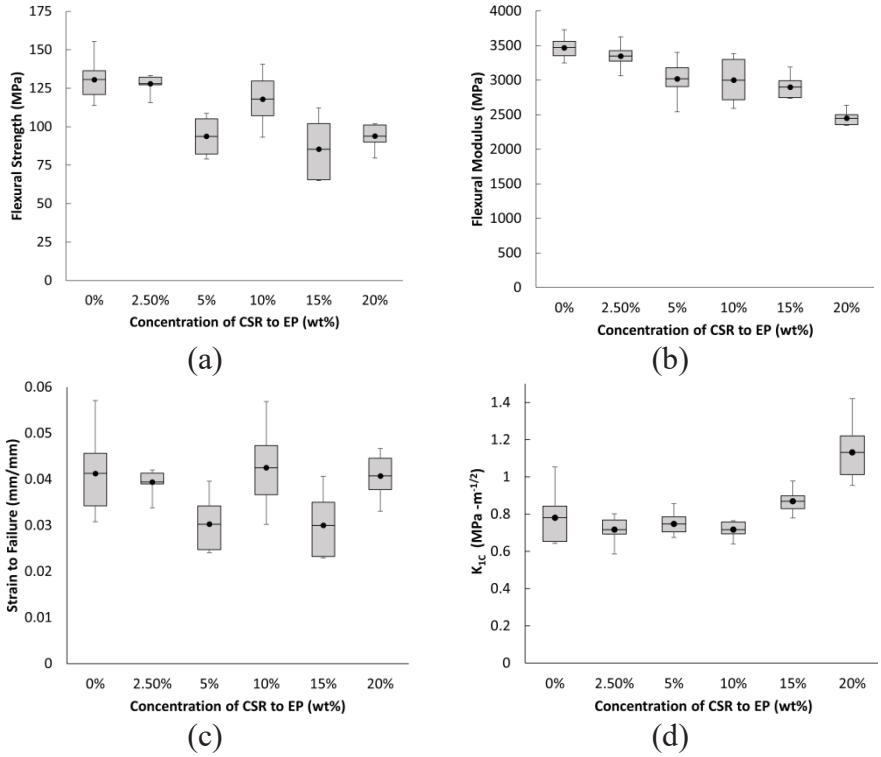

Figure 5 - Summary of flexural strength, modulus, and SENB fracture toughness for 0-20 wt% CSR modified neat resins

3.3 Acoustic Emission Spectroscopy of the Carbon Fibre Composites

Given the very good improvement in fracture toughness (K_{IC}) for the 20 wt% CSR modified epoxy network, the corresponding composite was fabricated and compared to the unmodified TGDDM/DDS composite to further understand the failure mechanism and explore the AE response.

AE sensors measure the voltage response from failure events that excite the sensor at a given frequency and above a threshold amplitude. In addition, the dataset for an event includes both a hit and a count. One event produces one hit and within that hit are one or many counts that represent the cumulative number of pulses above a certain amplitude. These hits and counts provide a partial description about the amount of AE activity that occurs and the relative shape of the acoustic waveform.

Examples of how the experimental load during crack propagation relates to the hit and count data measured from AE spectroscopy for an unmodified and CSR toughened composites therefore, are shown below in Figure 6.

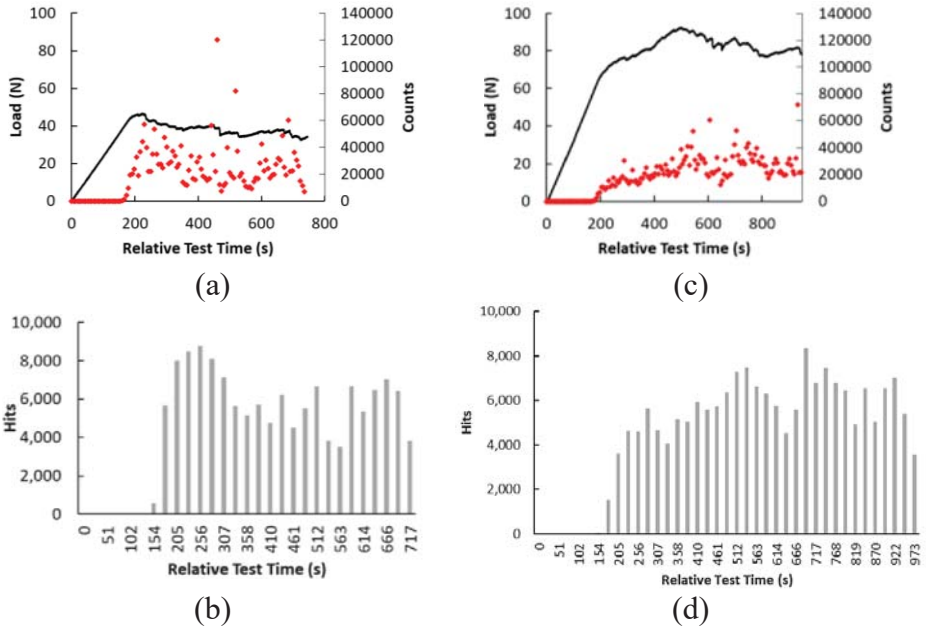

Figure 6 – Summary load profile (black), counts (red), and hits versus relative test time for (a-b), TGDDM-DDS Sample 1 and (c-d) TGDDM-DDS 20 wt% CSR Sample 5

The load versus time curves of the unmodified and 20 wt% CSR modified systems show quite different behaviour clearly reflected by their respective counts and hits. The unmodified resin shows a decaying load with increasing crack length which corresponds to a high number of hits at the start of the test but also decreases with crack length, indicating reduced acoustic activity during propagation. In contrast, the loading curve of the 20 wt% CSR system shows a series of events where the load increase, drops off, increases, and drops off yet merging around a median value. This behaviour is consistent with a stick-slip phenomena where the crack front is continually arrested along the length of the DCB test regime. Similarly, the hits tend to peak near the peak load and diminish after the intermittent drop in load and the counts tend to remain constant suggesting an accumulation of damage prior to unloading. These instances were often observed to occur in conjunction with a visually apparent bridging at the crack tip or a jump in crack tip location along the edge of the sample specimens.

The mean and peak frequencies of AE signals were determined for all AE-DCB tests relative to the lead and lag sensors and are shown in Figure 7. Here, the peak events tended to occur at slightly higher magnitudes for sensor 1 versus sensor 2 and are attributed to the initial distance of 55 mm between the lag sensor 2 and the crack tip. As the crack propagates a slight reduction in the difference between the signals is observed as the crack tip approaches sensor 2. For both the unmodified and CSR toughened laminates, the lower frequency (mean and peak) events (70-250 kHz) are the most common events throughout the test compared to the higher frequencies (250-550 kHz). Observation of the peak frequencies, highlight more clearly the differences in the AE response of the unmodified and toughened laminates. As can be seen in Figure 7(b) and (d), in the 250-550 kHz range, a two-fold increase in the peak frequency events occurring for the toughened laminates illustrates the greater number of energy dissipation events as would be expected for a toughened network. Typically, the test time of an unmodified laminate was 750 s while the toughened laminates were carried out to completion around 1000 s, further highlighting the enhanced resistance to crack propagation.

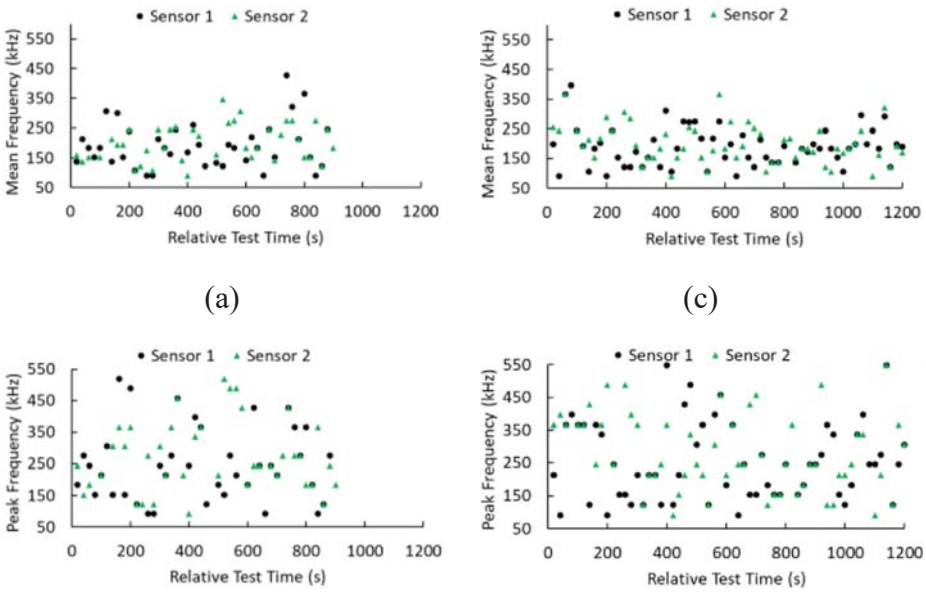

Figure 7 - Summary of mean and peak frequencies relative to test time for (a-b), TGDDM-DDS Sample 1 and (c-d) TGDDM-DDS 20 wt% CSR Sample 5

Previous work into the AE response of resins and composites emphasises the dependence of failure mechanisms on excitation frequency. While its not possible to specify the cut off frequences exactly, lower frequency events are associated primarily with matrix failure while higher frequencies are associated with fibre-matrix interactions and interply failures. Figure 8(a) and (b) plots the number of events measured by the mean and peak frequencies respectively, measured by AE for bands of 70-150 kHz, and in 100 kHz increments up to a maximum 550 kHz. The peaks occurred above a threshold voltage of 10mV. For both mean and peak frequencies, the most number of events occur in the 150-250 kHz range, still associated primarily with matrix failure. For the lower lower-frequency band (70-150 kHz), also likely to be matrix failure, the number of events between the unmodified and modified laminates are similar to each other. As the frequency bands increase from 150 to 550 kHz a higher number of peak events for the CSR toughened composites is observed. Clearly, increased matrix toughness is evident from the higher number of events at higher frequencies and reflects the importance of additional dissipation mechanisms related to fibre matrix and interply failure. Indeed peak frequencies above 250 kHz are associated with interply and fibre-dominated failure and correlate with the stick-slip behaviour observed during loading.

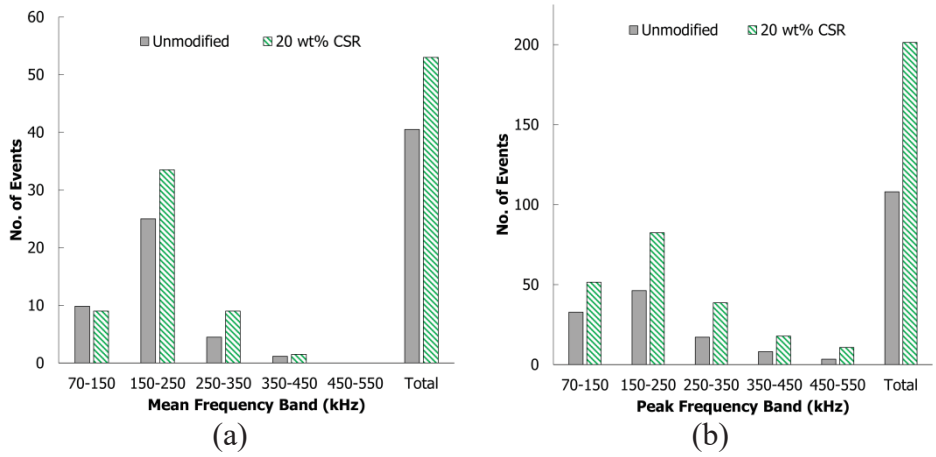

Figure 8 – Count of (a) mean frequencies and (b) peak frequency events per band for unmodified and 20 wt% CSR samples averaged across all AE tests.

The R-curves of the unmodified and 20 wt% CSR modified epoxy composites are shown in Figure 9 and illustrate the large improvement in fracture toughness. The results are presented in Table 4 for the mode I strain energy release rate and the cumulative AE energy. Fracture toughness of the unmodified composite was 211.8 J/m^2 but increased to 454.1 J/m^2 an increase of 114.7%, significantly higher than the 45% improvement at the same concentration for the neat resin. This

compares well with other studies which have ranged from improvements of 53-197% (K_{1C} and G_{1C}) using core shell rubber to toughen epoxy networks [19]–[24]. For example, Riew et al. observed a 78% improvement to G_{1C} in a formulation containing parts diglycidal ether of bisphenol A (DGEBA) and TGDDM cured with DDS [30].

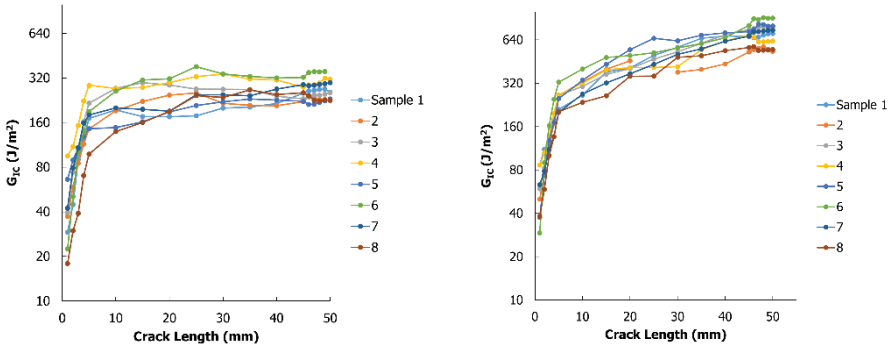

Figure 9 - Fracture toughness R-curves of (a) unmodified and (b) 20 wt% CSR laminates

Table 4 – Fracture toughness and cumulative AE energy

	G_{1C} Fracture Toughness (J/m^2)	Cumulative AE Energy (J)
Unmodified	211.8 (± 36.5)	1.59 (± .71)
20 wt% CSR	454.1 (± 64.6)	2.06 (± .86)
% Diff.	114.7	29.56

3.4 SEM Investigation of Failure Mechanisms

Scanning electron microscopy (SEM) was carried out on segments of the composite in the region of 5, 25, and 50 mm lengths from the initial pre-crack. Images of the fracture surface of a resin-rich region from a segment cut from the 25 mm region are shown in Figure 10(a) and (b) for the unmodified and modified composites respectively. The fracture surfaces of the neat resin (Figure 10(a)) display brittle behaviour consisting of smooth surfaces and sharp ordered striations. Further evidence of brittle failure of the resin is shown on the surface of the matrix and fibre. The CSR modified laminate in Figure 10(b) shows markedly different behaviour, consistent with more ductile failure. Extensive cavitation of sub-micron sized particles is evident and the striations observed in Figure 10(a) are more abundant and ragged, similar in appearance to a rubber toughened composite and consistent with crazing and cavitation behavior [56].

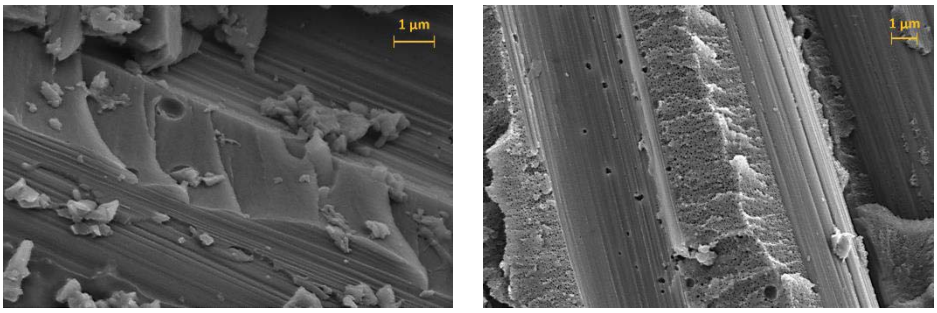

(a) (b)

Figure 10 - SEM fractograms of the (a) unmodified and (b) 20 wt% CSR toughened composites taken from a segment of the laminate at the 25mm region of the crack length

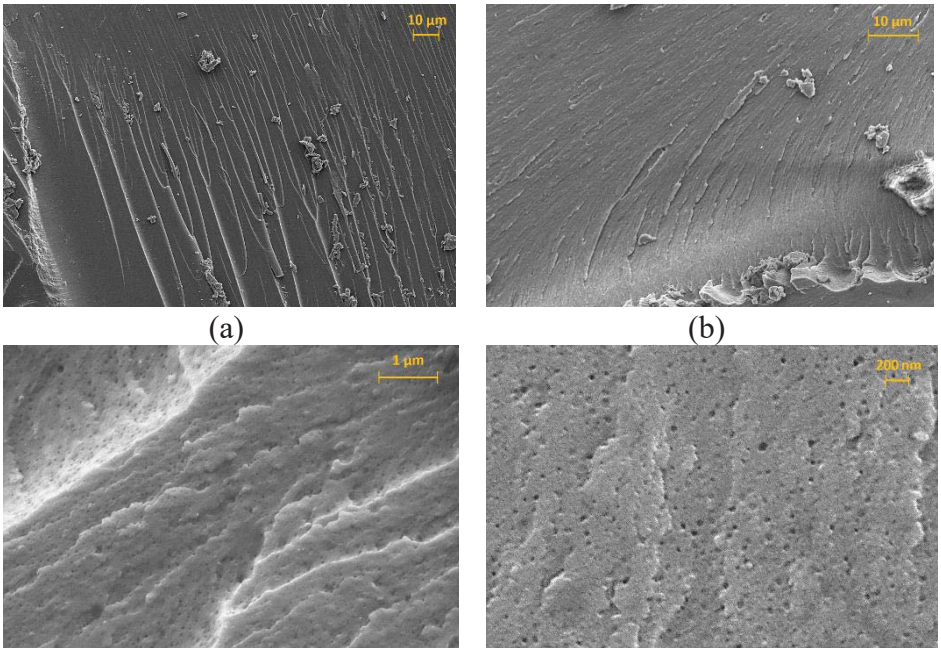

(a) (b)

(c) (d)

Figure 11 - SEM fractograms of the (a) unmodified and (b-d) 20 wt% CSR modified neat resins at different magnifications

With respect to the polymer network toughening, the effect of CSR addition is modest compared with other reported studies. The fracture surfaces of the unmodified network and selected images of the 20 wt% CSR modified network are shown Figure 11. The fracture surface of unmodified network shown in Figure 11(a) exhibits very brittle behavior and shows multiple parallel striations. Several images of the fracture surfaces of the 20 wt % CSR at various magnifications are shown in Figure 11(b)-(d) to illustrate the significant transformation from brittle to increasingly ductile behaviour. Extensive cavitation of sub-micron particles, stress whitening and shear band formation is evident. Importantly, and particularly evident in Figure 11(d) is the

excellent dispersion of the CSR with no evidence of large-scale agglomeration being apparent.

The large difference between the improvements in fracture of the neat resin and the composite may be attributed to a size effect described by Bagheri & Pearson [33], where they observed that thinner samples (1 mm) had higher toughness than thicker samples (max of 6 mm). The increase to toughness was also shown to follow a power law. Matrix-rich regions of the laminate have a much smaller aspect ratio. Also, CSR particles reduce the strength and stiffness of epoxy network. A combination of these two factors may contribute to the excellent improvement to the composite fracture toughness by CSR addition.

4 CONCLUSIONS

In summary, this study presents a CSR toughening study of a high T_g TGDDM/DDS network in neat polymer and composite form. Some key findings from this investigation are as follows:

1. CSR particles of a polybutadiene core and poly methyl methacrylate shell produce a modest increase in T_g and T_d of the cured network while decreasing the char yield and physical density.

2. CSR addition increases the cure reaction modestly while not affecting the chemistry to any significant degree, although the activation energy barrier increases with CSR addition.

3. Flexural modulus and strength all decrease with increasing CSR concentration while the strain to failure is unaffected.

4. Toughening (K_{IC}) of the neat resin was not observed for lower concentrations of CSR but achieved 11.4% and 45% improvement in fracture toughness at 15 wt% and 20 wt% CSR, respectively. The strain energy release rate (G_{IC}) displayed a 115% improvement for the 20 wt% CSR modified carbon fibre composite. Toughening mechanisms of the polymer and composite included cavitation and shear band formation.

5. Acoustic emission spectroscopy showed that the toughened matrix displayed significantly more AE events across a wide range of frequencies. This was particularly evident at higher frequencies and was attributed to the presence of additional fibre dominated toughening mechanisms operating.

Declaration of Competing Interests

This research did not receive any specific grant from funding agencies in the public, commercial, or not-for-profit sectors.

5 REFERENCES

[1] J.-P. Pascault and R. J. J. Williams, “General Concepts about Epoxy Polymers,” in *Epoxy Polymers*, Weinheim, Germany: Wiley-VCH Verlag GmbH & Co. KGaA, 2010, pp. 1–12.

[2] M. T. Demeuse, “Introduction to high temperature polymer blends,” in *High Temperature Polymer Blends*, Cambridge, United Kingdom: Woodhead Publishing, 2014, pp. 1–13.

[3] P. M. Hergenrother, “The Use, Design, Synthesis, and Properties of High Performance/High Temperature Polymers: An Overview,” *High Perform. Polym.*, vol. 15, no. 1, pp. 3–45, Mar. 2003, doi: 10.1177/095400830301500101.

[4] C.-S. Wang and M.-C. Lee, “Synthesis and modification of a naphthalene-containing trifunctional epoxy resin for electronic applications,” *J. Appl. Polym. Sci.*, vol. 70, no. 10, pp. 1907–1921, Dec. 1998, doi: 10.1002/(SICI)1097-4628(19981205)70:10<1907::AID-APP5>3.0.CO;2-Y.

[5] S. P. Rwei, C. Y. Cheng, G. S. Liou, and K. C. Cheng, “Curing and pyrolysis of cresol novolac epoxy resins containing BABODOPN,” *Polym. Eng. Sci.*, vol. 45, no. 4, pp. 478–486, Apr. 2005, doi: 10.1002/pen.20305.

[6] C. B. Bucknall, P. S. Heather, and A. Lazzeri, “Rubber toughening of plastics,” *J. Mater. Sci.*, vol. 24, no. 6, pp. 2255–2261, Jun. 1989, doi: 10.1007/BF02385450.

[7] D. . Hourston and J. . Lane, “The toughening of epoxy resins with thermoplastics: 1. Trifunctional epoxy resin-polyetherimide blends,” *Polymer (Guildf).*, vol. 33, no. 7, pp. 1379–1383, Jan. 1992, doi: 10.1016/0032-3861(92)90110-I.

[8] T. Liu *et al.*, “Nitrogen-Free Tetrafunctional Epoxy and Its DDS-Cured High-Performance Matrix for Aerospace Applications,” *Ind. Eng. Chem. Res.*, vol. 56, no. 27, pp. 7708–7719, Jul. 2017, doi: 10.1021/acs.iecr.7b00096.

[9] X. Cheng, Q. Wu, S. E. Morgan, and J. S. Wiggins, “Morphologies and mechanical properties of polyethersulfone modified epoxy blends through multifunctional epoxy composition,” *J. Appl. Polym. Sci*, vol. 134, 2017, doi: 10.1002/app.44775.

[10] Y. F. Yu, J. Cui, W. J. Chen, and S. J. Li, “Studies on the Phase Separation of Polyetherimide Modified Tetrafunctional Epoxy Resin. II. Effects of the Molecular Weight,” vol. 35, no. 1, pp. 121–135, 1998.

[11] A. Chandramohan and M. Alagar, “Synthesis and characterization of 1, 1-bis (3-methyl-4-epoxyphenyl) cyclohexane-toughened DGEBA and TGDDM organo clay hybrid nanocomposites,” *High Perform. Polym.*, 2011, doi: 10.1177/0954008310397634.

[12] D. S. Kim, M. J. Han, and J. R. Lee, “Cure behavior and properties of an epoxy resin modified with a bismaleimide resin,” *Polym. Eng. Sci.*, vol. 35, no. 17, pp. 1353–1358, 1995, doi: 10.1002/pen.760351705.

[13] J. Zhang, Q. Guo, and B. Fox, “Thermal and mechanical properties of a dendritic hydroxyl-functional hyperbranched polymer and tetrafunctional epoxy resin blends,” *J. Polym. Sci. Part B Polym. Phys.*, 2010, doi: 10.1002/polb.21902.

[14] E. Martuscelli, P. Musto, G. Ragosta, F. Riva, and L. Mascia, “Toughening of tetrafunctional (TGDDM) epoxy resins with telechelic extended perfluoroligomers,” *J. Mater. Sci.*, vol. 35, no. 15, pp. 3719–3726, 2000, doi: 10.1023/A:1004852624444.

[15] P. Musto, E. Martuscelli, G. Ragosta, P. Russo, and G. Scarinzi, “An interpenetrated system based on a tetrafunctional epoxy resin and a thermosetting bismaleimide: Structure-properties correlation,” *J. Appl. Polym. Sci.*, vol. 69, no. 5, pp. 1029–1042, Aug. 1998, doi: 10.1002/(SICI)1097-4628(19980801)69:5<1029::AID-APP23>3.0.CO;2-V.

[16] C. B. Bucknall and I. K. Partridge, “Phase separation in epoxy resins containing polyethersulphone,” *Polymer (Guildf).*, 1983, doi: 10.1016/0032-3861(83)90120-9.

[17] R. S. Raghava, “Role of matrix- particle interface adhesion on fracture toughness of dual phase epoxy- polyethersulfone blend,” *J. Polym. Sci. Part B Polym. Phys.*, 1987, doi: 10.1002/polb.1987.090250504.

[18] R. S. Raghava, “Development and characterization of thermosetting- thermoplastic polymer blends for applications in damage- tolerant composites,” *J. Polym. Sci. Part B Polym. Phys.*, 1988, doi: 10.1002/polb.1988.090260103.

[19] E. R. Mafi and M. Ebrahimi, “Role of core-shell rubber particle cavitation resistance on toughenability of epoxy resins,” *Polym. Eng. Sci.*, vol. 48, no. 7, pp. 1376–1380, Jul. 2008, doi: 10.1002/pen.21104.

[20] L. Becu, A. Maazouz, H. Sautereau, and J. F. Gerard, “Fracture behavior of epoxy polymers modified with core-shell rubber particles,” *J. Appl. Polym. Sci.*, vol. 65, no. 12, pp. 2419–2431, Sep. 1997, doi: 10.1002/(SICI)1097-4628(19970919)65:12<2419::AID-APP14>3.0.CO;2-W.

[21] K. T. Gam, M. Miyamoto, R. Nishimura, and H. J. Sue, “Fracture behavior of core-shell rubber-modified clay-epoxy nanocomposites,” *Polym. Eng. Sci.*, vol. 43, no. 10, pp. 1635–1645, Oct. 2003, doi: 10.1002/pen.10137.

[22] J. Chen, A. J. Kinloch, S. Sprenger, and A. C. Taylor, “The mechanical properties and toughening mechanisms of an epoxy polymer modified with polysiloxane-based core-shell particles,” *Polymer (Guildf).*, vol. 54, no. 16, pp. 4276–4289, Jul. 2013, doi: 10.1016/J.POLYMER.2013.06.009.

[23] D. Quan and A. Ivankovic, “Effect of core–shell rubber (CSR) nano-particles on mechanical properties and fracture toughness of an epoxy polymer,” *Polymer (Guildf).*, vol. 66, pp. 16–28, Jun. 2015, doi: 10.1016/J.POLYMER.2015.04.002.

[24] W. Wan, D. Yu, J. He, Y. Xie, L. Huang, and X. Guo, “Simultaneously improved toughness and dielectric properties of epoxy/core-shell particle blends,” *J. Appl. Polym. Sci.*, vol. 107, no. 2, pp. 1020–1028, Jan. 2008, doi: 10.1002/app.26102.

[25] D. S. Parker, H.-J. Suet, J. Huang, and A. F. Yee~, “Toughening mechanisms in core-shell rubber modified polycarbonate.”

[26] C. B. Bucknall, A. Karpodinis, and X. C. Zhang, “A model for particle cavitation in rubber-toughened plastics,” *J. Mater. Sci.*, vol. 29, no. 13, pp. 3377–3383, 1994, doi: 10.1007/BF00352036.

[27] J. U. Starke, R. Godehardt, G. H. Michler, and C. B. Bucknall, “Mechanisms of cavitation over a range of temperatures in rubber-toughened PSAN modified with three-stage core-shell particles,” *J. Mater. Sci.*, 1997, doi: 10.1023/A:1018556923774.

[28] D. S. Ayre and C. B. Bucknall, “Particle cavitation in rubber-toughened PMMA: Experimental testing of the energy-balance criterion,” *Polymer (Guildf).*, 1998, doi: 10.1016/S0032-3861(97)10253-1.

[29] C. B. Bucknall, “Applications of microscopy to the deformation and fracture of rubber-toughened polymers,” *J. Microsc.*, 2001, doi: 10.1046/j.1365-2818.2001.00838.x.

[30] C. K. Riew, A. R. Siebert, R. W. Smith, M. Fernando, and A. J. Kinloch, “Toughened Epoxy Resins: Preformed Particles as Tougheners for Adhesives and Matrices,” 1996, pp. 33–44.

[31] W. L. Bradley, W. Schultz, C. Corleto, and S. Komatsu, “The Synergistic Effect of Cross-Link Density and Rubber Additions on the Fracture Toughness of Polymers,” 1993, pp. 317–334.

[32] R. Bagheri and R. A. Pearson, “Role of particle cavitation in rubber-toughened epoxies: 1. Microvoid toughening,” *Polymer (Guildf).*, vol. 37, no. 20, pp. 4529–4538, Sep. 1996, doi: 10.1016/0032-3861(96)00295-9.

[33] R. Bagheri and R. A. Pearson, “Role of particle cavitation in rubber-toughened epoxies: II. Inter-particle distance,” *Polymer (Guildf).*, vol. 41, no. 1, pp. 269–276, Jan. 2000, doi: 10.1016/S0032-3861(99)00126-3.

[34] P. J. de Groot, P. A. M. Wijnen, and R. B. F. Janssen, “Real-time frequency determination of acoustic emission for different fracture mechanisms in carbon/epoxy composites,” *Compos. Sci.*

Technol., vol. 55, no. 4, pp. 405–412, Jan. 1995, doi: 10.1016/0266-3538(95)00121-2.

[35] M. Giordano, A. Calabro, C. Esposito, A. D'Amore, and L. Nicolais, "An acoustic-emission characterization of the failure modes in polymer-composite materials," *Compos. Sci. Technol.*, vol. 58, no. 12, pp. 1923–1928, Dec. 1998, doi: 10.1016/S0266-3538(98)00013-X.

[36] J. Bohse, "Acoustic emission examination of polymer-matrix composites," *J. Acoust. Emiss.*, no. 22, pp. 208–223, 2004.

[37] R. Gutkin, C. J. Green, S. Vangrattanachai, S. T. Pinho, P. Robinson, and P. T. Curtis, "On acoustic emission for failure investigation in CFRP: Pattern recognition and peak frequency analyses," *Mech. Syst. Signal Process.*, 2011, doi: 10.1016/j.ymssp.2010.11.014.

[38] A. J. Brunner, "Identification of damage mechanisms in fiber-reinforced polymer-matrix composites with Acoustic Emission and the challenge of assessing structural integrity and service-life," *Constr. Build. Mater.*, vol. 173, pp. 629–637, Jun. 2018, doi: 10.1016/J.CONBUILDMAT.2018.04.084.

[39] J. M. Berthelot and J. Rhazi, "Acoustic emission in carbon fibre composites," *Compos. Sci. Technol.*, vol. 37, no. 4, pp. 411–428, Jan. 1990, doi: 10.1016/0266-3538(90)90012-T.

[40] F. Lissek, A. Haeger, V. Knoblauch, S. Hloch, F. Pude, and M. Kaufeld, "Acoustic emission for interlaminar toughness testing of CFRP: Evaluation of the crack growth due to burst analysis," *Compos. Part B Eng.*, 2018, doi: 10.1016/j.compositesb.2017.10.012.

[41] N. Chandarana, D. Sanchez, C. Soutis, and M. Gresil, "Early Damage Detection in Composites during Fabrication and Mechanical Testing," *Materials (Basel).*, vol. 10, no. 7, p. 685, Jun. 2017, doi: 10.3390/ma10070685.

[42] C. Barile, C. Casavola, G. Pappalettera, and P. K. Vimalathithan, "Damage characterization in composite materials using acoustic emission signal-based and parameter-based data," *Compos. Part B Eng.*, vol. 178, p. 107469, Dec. 2019, doi: 10.1016/j.compositesb.2019.107469.

[43] A. K. Arnautov, O. Bikovens, V. Gribniak, A. Nasibullins, I. Blumbergs, and M. Hauka, "Investigation on fracture of epoxy-filled composites by acoustic emission," *J. Civ. Eng. Manag.*, 2016, doi: 10.3846/13923730.2016.1157094.

[44] ASTM Int., "Standard Test Methods for Flexural Properties of Unreinforced and Reinforced Plastics and Electrical Insulating Materials 1," *ASTM Int.*, 2003, doi: 10.1520/D0790-17.

[45] "Standard Test Methods for Plane-Strain Fracture Toughness and Strain Energy Release Rate of Plastic Materials 1," doi: 10.1520/D5045-14.

[46] "Standard Test Method for Mode I Interlaminar Fracture Toughness of Unidirectional Fiber-Reinforced Polymer Matrix Composites 1," doi: 10.1520/D5528-13.

[47] J. M. Barton and D. C. L. Greenfield, "Differential Scanning Calorimetry Cure Studies of Tetra-N-glycidyldiaminodiphenylmethane Epoxy Resins 3 - Reaction with Dicyandiamide," *Br. Polym. J.*, vol. 18, no. 3, pp. 196–200, May 1986, doi: 10.1002/pi.4980180311.

[48] J. Gonis, G. P. Simon, and W. D. Cook, "Cure properties of epoxies with varying chain length as studied by DSC," *J. Appl. Polym. Sci.*, vol. 72, no. 11, pp. 1479–1488, Jun. 1999, doi: 10.1002/(SICI)1097-4628(19990613)72:11<1479::AID-APP9>3.0.CO;2-E.

[49] L. Yang, C. Zhang, S. Pilla, and S. Gong, "Polybenzoxazine-core shell rubber–carbon nanotube nanocomposites," *Compos. Part A Appl. Sci. Manuf.*, vol. 39, no. 10, pp. 1653–1659, Oct. 2008, doi: 10.1016/J.COMPOSITESA.2008.07.004.

[50] S. R. Mousavi and I. Amiri Amraei, "Influence of nanosilica and methyl methacrylate–butadiene–styrene core–shell rubber particles on the physical-mechanical properties and cure kinetics of diglycidyl ether of bisphenol-A-based epoxy resin," *High Perform. Polym.*, vol. 28, no. 7, pp. 809–819, Sep. 2016, doi: 10.1177/0954008315600228.

[51] A. Maazouz, H. Sautereau, and J. F. Gerard, "Toughening of epoxy networks using pre-formed core-shell particles or reactive rubbers," *Polym. Bull.*, vol. 33, no. 1, pp. 67–74, Jun. 1994, doi: 10.1007/BF00313475.

[52] H. J. Sue, J. L. Bertram, E. I. Garcia-Meitin, J. W. Wilchester, and L. L. Walker, "Fracture behavior of core-shell rubber-modified crosslinkable epoxy thermoplastics," *Colloid Polym. Sci.*, 1994, doi: 10.1007/BF00659459.

[53] G. Giannakopoulos, K. Masania, and A. C. Taylor, "Toughening of epoxy using core-shell particles," *J. Mater. Sci.*, 2011, doi: 10.1007/s10853-010-4816-6.

[54] B. J. Cardwell and A. F. Yee, "Rate and temperature effects on the fracture toughness of a rubber-modified epoxy."

[55] D. R. Long, L. Conca, and P. Sotta, "Dynamics in glassy polymers: The Eyring model revisited," *Phys. Rev. Mater.*, vol. 2, no. 10, p. 105601, Oct. 2018, doi: 10.1103/PhysRevMaterials.2.105601.

[56] J. Y. Lee, I.-J. Chin, and J. Choi, "Effect of particle size and crosslinking on the toughening of core-shell-type rubber-modified poly(lactic acid) composites," 2018, doi: 10.1016/j.polymertesting.2017.12.028.